PAPER

Check for updates

High dispersions of nano zero valent iron supported on biochar by one-step carbothermal synthesis and its application in chromate removal

Shifeng Li, [ID] *[ab] Tingting You,[a] Yang Guo,[a] Shuhua Yao,[a] Shuyan Zang,*[a] Min Xiao,[c] Zhigang Zhang[d] and Yanming Shen[d]

A one-step carbothermal synthesis and characterization of biochar-supported nanoscale zero-valent iron (nZVI/BC) was performed for the removal of hexavalent chromium (Cr(VI)) from aqueous solution. High dispersions of nanoscale zero-valent iron supported on biochar were successfully synthesized by the pyrolysis of an iron-impregnated biomass (corn stover) as the carbon and iron source under nitrogen atmosphere. The effects of the pyrolytic temperature on the Fe mineralogies formed on the biochar are discussed. In general, the effects of the treatment time, initial solution pH, and nZVI/BC dosage on the Cr(VI) removal are presented. The results showed high crystallinity and purity, and nZVI/BC was obtained at a pyrolytic temperature of 800 °C. The batch experimental results determined that the adsorption capacity of Cr(VI) decreases with the increase in the initial pH value from 4.0 to 10.0. The Cr(VI) adsorption kinetics data effectively followed a pseudo-second-order kinetics with a calculated rate constant of 0.0.3396 g mg^{-1} min^{-1}. The calculated thermodynamic parameters, such as $\Delta G°$, $\Delta H°$, and $\Delta S°$, were evaluated, and the results indicated that the Cr(VI) reduction on nZVI/BC was a spontaneous and endothermic process. The adsorption mechanism of Cr(VI) was investigated by XRD and XPS analyses and the results demonstrated that Cr(VI) was reduced to Cr(III) and the oxidation of nZVI occurred during the reaction process. These results prove that nZVI/BC synthesized by a one-step carbothermal method can be considered as a potential candidate for the removal of Cr(VI) from aqueous solutions.

1 Introduction

Chromium (Cr), one of the most abundant contaminants found in the environment, especially in water and soil, is mainly a byproduct of electroplating, ore mining, leather tanning, pigment making *etc.*[1] In natural aquatic environments, Cr(VI) and Cr(III) are the predominant forms of chromium. In general, Cr(III) occurs naturally and is an essential micronutrient for humans. However, Cr(VI) is regarded to be toxic and potentially carcinogenic.[2] Therefore, the treatment of Cr(VI)-containing wastewater has become a booming research area.

Considerable research efforts have been focused on various methods of removal of Cr(VI) from Cr(VI)-containing wastewater, including adsorption, ion exchange, flotation, coagulation,

membrane technologies and chemical reduction.[3–8] Among these technologies, the removal of Cr(VI) by nZVI, which has a large surface area and a high chemical reduction has been thought as a suitable process.[9] However, there are still some limitations that need to be addressed, especially when the nZVI particles tend to agglomerate and passivate in the surface during use.[10] To stabilize the as-synthesized iron nanoparticles, several materials have been investigated as supports, such as SiO$_2$,[11] montmorillonite,[12] resin,[13] activated carbon[14] and biochar.[15–18] Among these materials, biochar is used extensively for environmental application because it can be easily obtained from many kinds of waste biomass and can be produced at relatively low-cost.[5,16,19,20] Despite recent advances in the environmental applications of nZVI/BC, there remain numerous challenges that limit its practical use.[21,22] It is well known that most preparation procedures using nZVI/BC can be divided into two steps. First, biochar is prepared by combusting biomass under low oxygen conditions (pyrolysis). Then, ferric salt is loaded onto the biochar followed by reduction using borohydride to produce zero-valent iron nanoparticles on the biochar support. Therefore, such procedures are not only costly but also potentially cause secondary contamination to the environment (such as the discharge of borate-containing wastewater).[21]

[a] *Liaoning Engineering Research Center for Treatment and Recycling of Industrially Discharged Heavy Metals, Shenyang University of Chemical Technology, Shenyang 110142, China. E-mail: li.shi.feng@163.com; zangshuyan@126.com*

[b] *Key Laboratory of Pollution Ecology and Environmental Engineering, Institute of Applied Ecology, Chinese Academy of Sciences, Shenyang 110016, China*

[c] *School of Environment, Key Laboratory of Regional Environment and Eco-Remediation, Ministry of Education, Shenyang University, 110044 Shenyang, Liaoning, China*

[d] *Liaoning Provincial Key Laboratory of Chemical Separation Technology, Shenyang University of Chemical Technology, Shenyang 110142, China*

One-step pyrolysis can be an alternative method for nZVI/BC or Fe-oxide/BC preparation for the applications in environmental remediation.[21,23–26] Liu et al.[24] reported the synthesis of nZVI/C composites from natural hematite and sawdust via a one-step pyrolysis method. The composite showed good potential application in the adsorption of U(VI) from aqueous solutions. Wang et al.[26] prepared Fe and Zn oxides supported by biochar through a one-step pyrolysis at 600 °C and used it successfully for the removal of p-nitrophenol in wastewater. He et al.[23] also prepared iron oxide supported on biochar via a one-step thermal pyrolysis (600 °C) of corn straw impregnated with $FeCl_3$ solution, and then investigated the arsenate removal performance and mechanisms. Lawrinenko et al.[21] found that some biomass, such as corn stover and cellulose, pre-treated with $FeCl_3$ could effectively reduce Fe to ZVI at 900 °C. Nonetheless, the structural characteristics of composites (the formation of nZVI/BC or Fe-oxides/BC) at different pyrolysis temperatures and the treatment of other heavy metals (such as Cr(VI)) still require further investigation.

In this study, a one-step carbothermal synthesis method was developed to prepare nZVI/BC composites at different temperatures for chromate removal. The objectives of this study were (1) to prepare nZVI/BC composites at different temperatures and to investigate the structural characteristics of the composite using XRD, N_2 adsorption–desorption, TEM, and XPS; (2) to investigate the adsorption and desorption kinetics and thermodynamic behaviour of Cr(VI) on the nZVI/BC composite using the batch equilibration method; and (3) to propose the potential adsorption mechanisms for Cr(VI) by the nZVI/BC composite.

2 Materials and methods

2.1 Chemicals

All reagents were of analytical grade except hydrochloric acid (guaranteed reagent) and were used directly without further purification. Hydrochloric acid, ferric chloride hexahydrate, sulfuric acid, phosphoric acid, sodium hydroxide, potassium dichromate, and diphenylcarbazide were purchased from Sinopharm (China). 500 mg L^{-1} Cr(VI) standard solutions were purchased from Aladdin (China). Ultrapure water (Millipore) was used in our study.

2.2 Synthesis of nZVI/BC

The nZVI/BC was prepared by a one-step carbothermal synthesis method by the following procedure: first, the corn stover was ground, dried naturally, and filtered through a sieve having a 100-mesh (0.15 mm). Then a mixture of 1 g corn straw powder and a solution containing 0.405 g $FeCl_3 \cdot 6H_2O$ and 40 mL ultrapure water was stirred for 24 h, and dried at 80 °C for 72 h in an air-dry oven. Finally, the pre-treated corn straw was pyrolyzed for 2 h at 800 °C with a heating rate of 5 °C min^{-1} in a tube furnace under 80 mL min^{-1} nitrogen flow. The resulting nZVI/BC was ground and passed through a sieve having 200-mesh (0.074 mm) without further treatment.

2.3 Characterizations

XRD patterns of the pyrolysis products were recorded using a Bruker D8 Advance XRD diffractometer (Cu Kα, 40 kV and 40 mA, λ = 1.5406 Å). The BET measurements were performed and the pore-size distribution was evaluated using a Quantachrome Autosorb 1-C adsorption instrument. The morphology of the sample surface was observed by TEM (FEI Tecnai G2 F20) and FE-SEM (S4800 HITACHI). An X-ray photoelectron spectrometer (Thermo Scientific 250Xi, Al Ka, $h\nu$ = 1486.6 eV, 15 kV and, 10 mA) was used for the determination of the chemical states of the surface Cr and Fe elements. The Cr(VI) concentration was detected using a UV-Vis spectrophotometer (Shimadzu UV2550). Total Fe content in nZVI/BC was analysed by an atomic absorption spectrometer (Shimadzu AA6880).

2.4 Cr(VI) adsorption procedures

2.4.1 Effect of nZVI/BC dosage. In this study, the addition of nZVI/BC in the range of 0.025–2 g L^{-1} revealed the effect of nZVI/BC dosage on the Cr(VI) removal. The initial Cr(VI) concentration was set as 10 mg L^{-1}, and the pH value was set to 4.0 at 25 °C.

2.4.2 Effect of pH. A given dose of the Cr(VI) solution was added into the pre-treated nZVI/BC suspension, and the pH value was adjusted in advance in the range of 4.0–10.0 by NaOH and HCl. After the reaction, the suspension was centrifugally separated, and then passed through a 0.45-micron filter. The Cr(VI) in the filtrate was diluted to the appropriate concentrations, and then analysed on a UV-Vis spectrophotometer (λ = 540 nm).

2.4.3 Kinetic and thermodynamic procedures. In the kinetic experiment, the nZVI/BC (1.5 g L^{-1}) reacted with the Cr(VI) solution (750 mL, 10 mg L^{-1}) at pH 4.0 and ambient temperature. At different intervals, a solution was taken out of the suspensions, centrifugally separated, and passed through a 0.45-micron filter membrane, and then analysed using a UV-Vis spectrophotometer.

2.5 Adsorption kinetics study

The adsorption kinetics process can be described by pseudo-first-order,[27] pseudo-second-order,[28] Elovich,[29] and intraparticle diffusion[30] models. The equation for the pseudo-first-order kinetics model is expressed as

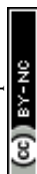$$\log(Q_e - Q_t) = \log Q_e - \frac{k_1}{2.303}t \tag{1}$$

where k_1 (min^{-1}) is the pseudo-first-order rate constant, and Q_e (mg g^{-1}) and Q_t (mg g^{-1}) are the adsorption capacities of Cr(V) at equilibrium and at time t (min), respectively.

The pseudo-second-order rate equation can be expressed as

$$\frac{t}{Q_t} = \frac{1}{k_2 Q_e^2} + \frac{t}{Q_e} \tag{2}$$

where k_2 (g mg^{-1} min^{-1}) is the pseudo-second-order rate constant.

The Elovich kinetics equation can be represented as

$$Q_t = a + b \ln t \tag{3}$$

where a (mg g^{-1}) and b (mg g^{-1}) are the Elovich adsorption kinetics constants.

The intraparticle diffusion model is expressed as

$$Q_t = k_p t^{0.5} + C \tag{4}$$

where k_p (mg g^{-1} min$^{-0.5}$) is the intraparticle diffusion rate constant.

2.6 Adsorption isotherm study

The Langmuir model is suitable for describing uniform adsorption processes, where each adsorption site on the surface of the sorbent is identical and the adsorption process is thought as monolayer adsorption. The Langmuir model can be expressed by the following eqn (5).[31]

$$\frac{C_e}{Q_e} = \frac{1}{Q_m b} + \frac{C_e}{Q_m} \tag{5}$$

where C_e (mg L^{-1}) is the adsorbate equilibrium ion concentration in solution and Q_e (mg g^{-1}) is the equilibrium amount of adsorbed ions on the sorbent, b (L mg^{-1}) is the Langmuir isotherm constant related to the energy of the sorbent, and Q_m (mg g^{-1}) is the calculated maximum adsorption capacity for a monolayer coverage. The adsorption on a heterogeneous surface can be described empirically by the Freundlich model and can be represented by the following eqn (6).[32]

$$\log Q_e = \log K_F \frac{1}{Q_m b} + \frac{1}{n} \log C_e \tag{6}$$

where K_F (L mg^{-1}) is the Freundlich affinity coefficient, and n is the Freundlich constant.

2.7 Thermodynamic study

The information on the energy change during the treatment of the Cr(VI)-containing aqueous solution by nZVI/BC can be provided by the thermodynamic equilibrium constant (K) under different temperatures.[33,34] First, the standard Gibbs free energy ΔG° (kJ mol^{-1}) can be obtained from the parameter K (eqn (7)). Then, the standard enthalpy change ΔH° (kJ mol^{-1}), and the standard entropy change ΔS° (J mol^{-1} K^{-1}) were calculated from the slope and intercept of the linear plot of $\ln K$ vs. $1/T$, respectively, where R is the universal gas constant (8.314 J mol^{-1} K^{-1}), and T is the solute temperature (K).

$$\Delta G^\circ = -RT \ln K \tag{7}$$

$$\ln K = \frac{\Delta S^\circ}{R} - \frac{\Delta H^\circ}{RT} \tag{8}$$

3 Results and discussion

3.1 Characterization of nZVI/BC

As we know, the pyrolytic temperature can influence the Fe mineralogies that form in the biochar.[21] As a result,

a temperature in the range of 600–900 °C was set during the pyrolysis process. The X-ray diffraction spectra of the pyrolysis products are shown in Fig. 1. In Fig. 1a, the diffraction peaks at 35.3°, 56.8°, and 62.3° 2θ are attributed to the (311), (511), and (440) characteristic diffraction peaks of magnetite (JCPDS no. 19-0629), respectively, indicating that magnetite but not ZVI was formed at 600 °C. As illustrated in Fig. 1(b and c), the (110), (200), and (211) characteristic diffraction peaks of the zero valent iron can be found at 44.6°, 65.0°, and 82.3° (JCPDS no. 06-0696) respectively, suggesting the presence of zero valent iron in the pyrolysis products.[25] Obviously, in the pyrolysis products at 800 °C and 900 °C, Fe(III) derived from ferric chloride was transformed to zero valent iron with high and sharp XRD diffraction peaks. However, the observation of no zero valent iron formation at 600 °C indicated that the pyrolysis temperature of 600 °C was not enough. The reaction equation is described as follows:[25]

$$2FeCl_3 \cdot 6H_2O = Fe_2O_3 + 6HCl\uparrow + 3H_2O\uparrow \tag{9}$$

$$2Fe_2O_3 + 3C = 4Fe + 3CO_2\uparrow \tag{10}$$
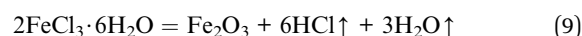
Thus, in this study the pyrolysis temperature was set as 800 °C.

The N$_2$ adsorption–desorption isotherm and the DFT pore diameter distribution of the nZVI/BC and BC prepared by pyrolysis at 800 °C are illustrated in Fig. 2. The adsorption–desorption isotherm curves of the nZVI/BC and BC can be categorized as type IV, and the H3 type hysteresis loop shows the mesoporous characteristics of the nZVI/BC composite.[35] Based on the isotherm of the N$_2$ adsorption and desorption, the calculated BET surface area for the nZVI/BC and the BC are 224.8 m^2 g^{-1} and 339.6 m^2 g^{-1}, respectively. The decrease in the BET surface area for nZVI/BC could be caused by the occupation of some of the pore space within BC. As shown in Fig. 2b, the most probable pore size for nZVI/BC is located at about 1.84 nm.

The typical FE-SEM image for BC (a) and the TEM image for nZVI/BC (b) are presented in Fig. 3. As shown in Fig. 3a, BC shows a smooth and compact surface morphology. Fig. 3b
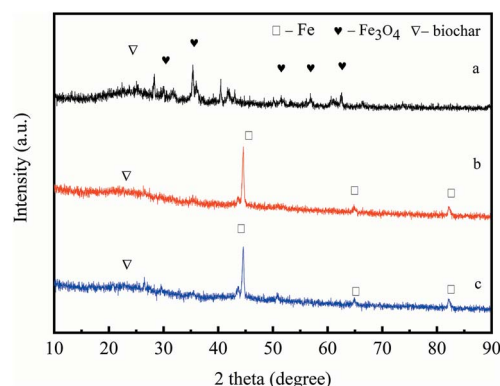

Fig. 1 XRD diffraction patterns of the nZVI/BC (or Fe$_3$O$_4$/BC) prepared by pyrolysis at 600 °C (a), 800 °C (b) and 900 °C (c), respectively.
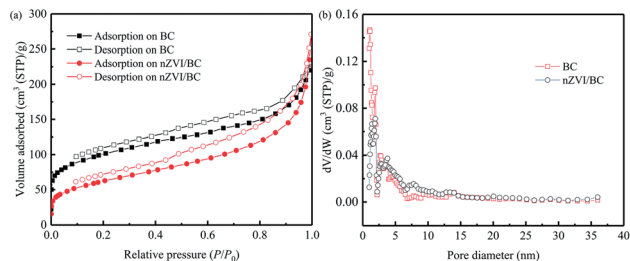
Fig. 2 N$_2$ adsorption/desorption isotherm (a) and the DFT pore diameter distribution (b) of the BC and the nZVI/BC.
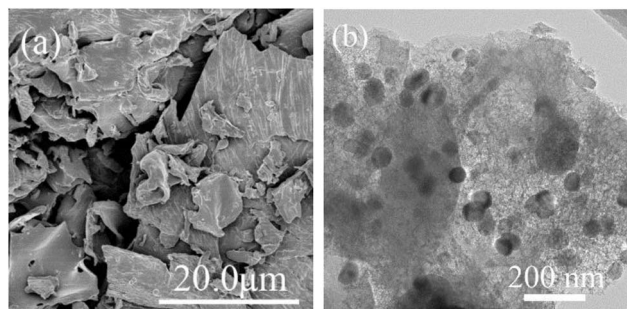

Fig. 3 Scanning electron microscopy morphology of BC (a) and transmission electron microscopy image of the nZVI/BC (b).

indicates that the zero valent iron particles with a diameter of about 50 nm were well-dispersed on the biochar, demonstrating that the agglomeration of nZVI particles was successfully prevented in the presence of biochar during pyrolysis. Moreover, the total Fe content in nZVI/BC composites as determined by AAS is 12.5 wt%.

3.2 Cr(vi) removal capacity

Fig. 4 shows that the removal capacity of Cr(vi) varies with different nZVI/BC dosages after 240 min treatment at ambient temperature. As we can see in Fig. 4, the removal capacity rises with the increase in the nZVI/BC dosage. For example, about
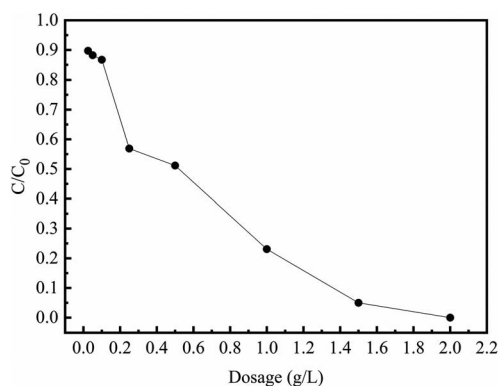

Fig. 4 The Cr(vi) removal at different nZVI/BC dosages (C$_0$: 10 mg L^{-1}; initial pH: 4.0; T: 25 °C).
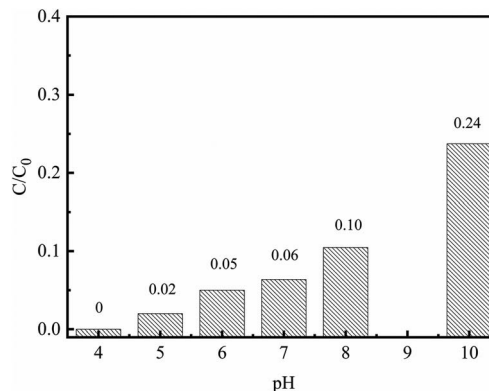

Fig. 5 The effect of the initial pH on Cr(vi) removal (C$_0$: 10 mg L^{-1}; nZVI/BC dosage: 1.5 g L^{-1}; T: 25 °C).

more than 96% of Cr(v) was removed with the nZVI/BC dosage of 1.5 g L^{-1}.

The effect of the initial pH on the removal capacity of Cr(vi) is shown in Fig. 5. It was found that the removal capacity of Cr(vi) was apparently affected by the pH in the range of 4.0–10.0. The Cr(vi) removal percentage declined from 100% to 76% with the solution pH increasing from 4 to 10. At pH ∼ 4.0, HCrO$_4^-$ is the main form of the Cr(vi), while CrO$_4^{2-}$ and Cr$_2$O$_7^{2-}$ are present mainly when the pH value varies from 8.0 to 10.0.[33] Therefore, at high solution pH, the strong competition between the Cr(vi) species and the hydroxyls (OH$^-$) should be the main reason for the low Cr(vi) removal capacity. In addition, the lower pH could contribute to the removal of the passive iron oxide layer, which covers the surface of nZVI and results in fresh nZVI being exposed to the surrounding Cr(vi) solution.[33] Hence, the initial pH of the Cr(vi) solution was set as 4.0 in all subsequent procedures.

3.3 Adsorption kinetics of Cr(vi)

Fig. 6 shows the adsorption kinetics of Cr(vi) on the nZVI/BC and BC. As can be seen from Fig. 6, in the presence of BC, the Cr(vi) concentration reduces slightly in the first 30 min. However, with nZVI/BC as the sorbent, the Cr(vi) concentration
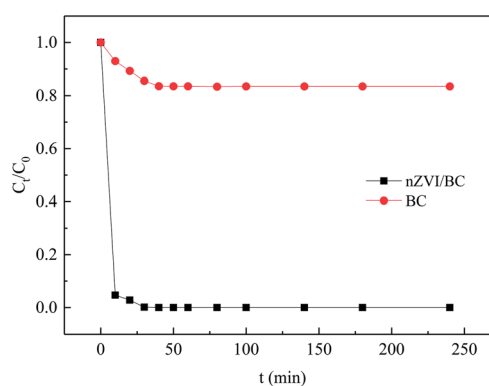

Fig. 6 The adsorption kinetics of Cr(vi) on the nZVI/BC and BC (C$_0$: 10 mg L^{-1}; sorbent dosage: 1.5 g L^{-1}; pH: 4.0; T: 25 °C).
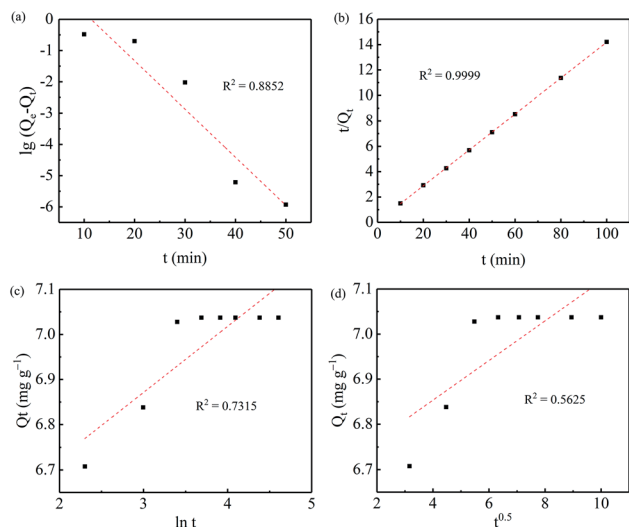
Fig. 7 The plots of the pseudo-first-order (a), pseudo-second-order (b), Elovich (c) and intraparticulate diffusion (d) models for the adsorption of Cr(VI) on the nZVI/BC.

Table 1 The adsorption kinetics parameters of Cr(VI) on the nZVI/BC

Model	Parameters	
Pseudo-first-order	k_1 (min^{-1})	0.3548
	Q_e (mg g^{-1})	56.51
	R^2	0.8852
Pseudo-second-order	k_2 (mg g^{-1} min^{-1})	0.3396
	Q_e (mg g^{-1})	7.08
	R^2	0.9999
Elovich	a (mg g^{-1})	6.43
	b (mg g^{-1})	0.15
	R^2	0.7315
Intraparticle diffusion	k_p (mg g^{-1})	0.043
	C	6.68
	R^2	0.5625

intraparticle diffusion models. As shown in Fig. 7 and Table 1, the kinetics data for the Cr(VI) adsorption were better fitted into the pseudo-second-order model ($R^2 = 0.9999$) than the other models.

Comparisons of the Cr(VI) adsorption kinetics rate constants of nZVI and other supported nZVI are summarized in Table 2. The results show that the nZVI/BC prepared by a one-step pyrolysis exhibited the highest adsorption rate for Cr(VI) than the related adsorbents reported in literature.

3.4 Thermodynamic analysis

In this study, we also studied the thermodynamic characteristics of the Cr(VI) removal procedures. The Cr(VI) adsorption isotherms are shown in Fig. 8 and fitted by the Langmuir and Freundlich isotherm model (Fig. 9). As shown in Fig. 9 and Table 3, the thermodynamic data for the Cr(VI) adsorption process fitted well to the Langmuir model.

The standard Gibbs free energy (ΔG°, kJ mol^{-1}) for Cr(VI) adsorption on the nZVI/BC can be calculated by eqn (7). Then, the standard enthalpy change (ΔH°, kJ mol^{-1}) and standard entropy change (ΔS°, J mol^{-1} K^{-1}) can be calculated according to eqn (8) by plotting ln K versus $1/T$ (Fig. 10). The results for the thermodynamic parameters are listed in Table 4. As shown in Table 4, ΔH° and ΔS° are positive and the ΔG° is negative, which indicates that the Cr(VI) adsorption on the nZVI/BC is thermodynamically endothermic and spontaneous. The thermodynamic analysis shows that the treatment of a Cr(VI)-containing aqueous solution with nZVI/BC is spontaneous and a high temperature is more favorable.[33,34]

As listed in Table 5, the maximum Cr(VI) adsorption capacity for nZVI at 298 K was compared to other related adsorbents reported in literatures. It can be seen that the Cr(VI) adsorption capacity on the nZVI/BC synthesized via a one-step pyrolysis is often higher than most nZVI sorbents prepared by liquid reduction.

3.5 Adsorption mechanisms of Cr(VI)

In this study, both XRD and XPS were applied to analyse the nZVI/BC after treatment with a Cr(VI) solution to reveal the mechanisms. After reacting with the Cr(VI) solution for 2 h, the XRD patterns of the nZVI/BC was not significantly changed (Fig. 11). However, compared to the freshly prepared nZVI/BC, iron oxide crystalline phases were distinctly detected. As shown in Fig. 11b, the diffraction peaks at 28.2°, 35.5°, and 62.5°, could be attributed to the characteristic diffraction peaks

decreases rapidly from 10 to 0.046 mg L^{-1} in the first few minutes and then reaches equilibrium (near 0) after 30 min. This result shows that the adsorption capacity of Cr(VI) on the BC is far below that on the nZVI/BC, which also can be deduced by the compact surface morphology and low specific surface area of BC (Fig. 2 and 3). The kinetics of the adsorption process on nZVI/BC was also fitted by different kinetics models such as the pseudo-first-order, pseudo-second-order, Elovich and

Table 2 Comparison of Cr(VI) adsorption kinetics rate constant of the nZVI related adsorbents[a]

Sorbent	Initial Cr(VI) concentration (mg L^{-1})	pH	Adsorption kinetics parameter (g mg^{-1} min^{-1})	Ref.
nZVI/AC[a]	10	5.0	0.0150	36
nZVI/zeolite[a]	50	7.0	0.0130	37
nZVI/BC[a]	10	—	0.1905	17
nZVI/BC[b]	10	4.0	0.3396	This study

[a] nZVI synthesis method: a, liquid reduction; b, one-step pyrolysis.
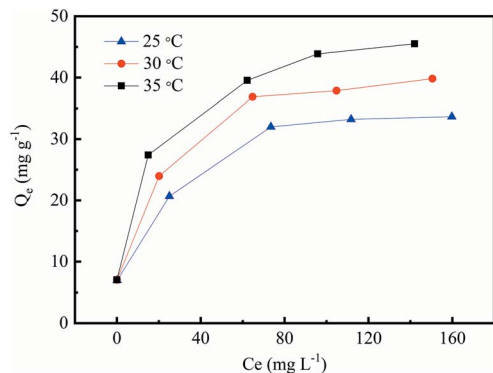
Fig. 8 Cr(VI) adsorption isotherms on the nZVI/BC (nZVI/BC dosage: 1.5 g L^{-1}; pH: 4.0; T: 25, 30 and 35 °C).

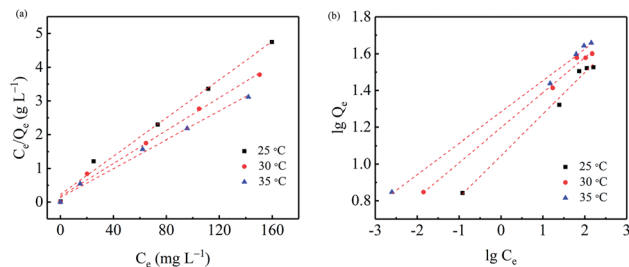**Fig. 9** Plots of the Langmuir isotherm model (a) and the Freundlich isotherm model (b) for the removal of Cr(VI) ions with nZVI/BC (T = 25 °C, pH = 4.0, nZVI/BC dosage = 1.5 g L^{-1}).

Table 3 The adsorption isotherm parameters of Cr(VI) on the nZVI/BC

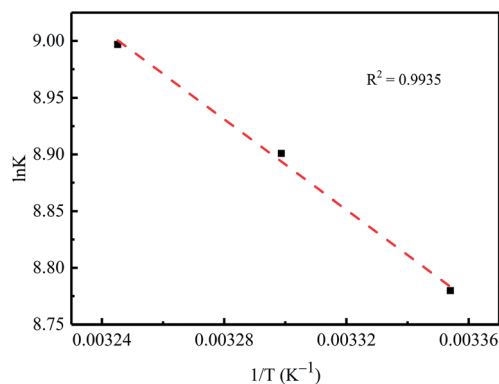| Model	Parameters	Temperature (°C)		
		25	30	35
Langmuir	b (g L^{-1})	0.125	0.141	0.155
	Q_m (mg g^{-1})	35.30	41.00	46.73
	R^2	0.988	0.990	0.994
Freundlich	K_F (L mg^{-1})	11.09	15.74	19.19
	$1/n$	0.226	0.191	0.170
	R^2	0.984	0.986	0.988

Fig. 10 0Variation of equilibrium constant K as a function of temperature (1/T).

Table 4 Thermodynamic parameters of Cr(VI) adsorption on the nZVI/BC

T/K	ln K	$\Delta G°$ (kJ mol^{-1})	$\Delta H°$ (kJ mol^{-1})	$\Delta S°$ (J mol^{-1} K^{-1})
298.15	8.780	−21.76	16.59	128.67
303.15	8.901	−22.44		
308.15	8.997	−23.05		

of FeOOH, Fe$_2$O$_3$ or Fe$_3$O$_4$, which were not clearly observed in the nZVI/BC before contacting with the Cr(VI) solution. In addition, the diffraction peaks at 36.2° and 55.5° could be derived from the (110) and (116) characteristic diffraction peaks of Cr$_2$O$_3$ (JCPDS no. 38-1479), respectively.[39,40] As a result, it can be deduced from Fig. 8 that Cr(VI) could be reduced to Cr(III) in Cr$_2$O$_3$(s) or the Cr(OH)$_3$(s) form and Fe^0 could be oxidized to FeOOH, Fe$_2$O$_3$, and Fe$_3$O$_4$.[39,41,42]

To further demonstrate the composition of the product, XPS analysis was performed. Compared with the freshly prepared nZVI/BC, after treatment with the Cr(VI) solution two new peaks appeared in curve i of Fig. 12a. As shown in Fig. 12b, there are two peaks at 586.8 eV (Cr 2p$_{1/2}$) and 577.3 eV (Cr 2p$_{3/2}$) after the reaction, indicating that Cr(III) compounds such as CrOOH, Cr(OH)$_3$, and Cr$_2$O$_3$ were the main chromium species on the surface.[33,43,44] Fig. 12c demonstrates the detailed curve-fitting spectra of the Fe 2p. The Fe 2p peaks at 710.4 eV and 711.8 eV can be assigned to Fe 2p$_{3/2}$ for Fe$_2$O$_3$ and/or FeOOH and Fe$_3$O$_4$. The peak at a binding energy of 725.0 eV indicated the existence of both Fe(II) and Fe(III) (Fe$_3$O$_4$ and/or FeOOH).[43-46] In addition, the peaks at 714.6, 718.9, and 733.4 eV can be ascribed to the satellite peaks of the Fe(II) and Fe(III) compounds.[47] The XRD and XPS results demonstrate that Cr(VI) could be reduced to Cr(III), while and nZVI could be oxidized to Fe(II) and Fe(III) compounds during the Cr(VI) removal.

3.6 Prospects and challenges

Nano zero valent iron (nZVI) has been shown to be an inexpensive and environmentally friendly material that can be applied to remediate many environmental contaminants (e.g. organic and heavy metal pollution). The pyrolysis of inexpensive and renewable biomass and iron salt should potentially be a greener and more sustainable pathway to produce the nZVI/BC sorbent for environmental remediation.[21] Although the batch experiment results have shown that the nZVI/BC exhibited an excellent Cr(VI) adsorption capacity, batch processing is generally not appropriate for industrial applications. The optimal adsorption process on a large scale should be dynamic (continuous flow mode) adsorption. In this study, the powdered nZVI/BC could present appreciable problems for column adsorption, so the next step will be to focus on studying the preparation of the granular sorbent and to study the adsorption capacity for pollution in continuous flow mode. Another challenge should be to reduce the energy consumption for the nZVI/BC synthesis process under higher temperature. Pyrolysis under a reducing atmosphere (e.g. CO or H$_2$) should be a potential pathway.

Table 5 Comparison of the maximum Cr(VI) adsorption capacity among nZVI and other related adsorbents

Sorbent	Preparation method	Initial pH	Adsorption capacity (mg g^{-1})	Ref.
nZVI	Liquid reduction	3.0	17.61	38
nZVI/BC	Liquid reduction	4.0	40.00	17
nZVI/zeolite	Liquid reduction	7.0	2.49	37
nZVI/BC	One-step pyrolysis	4.0	35.30	This work
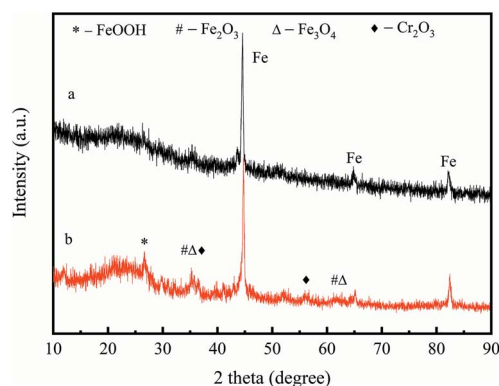
Fig. 11 XRD diffraction patterns for the nZVI/BC before (a) and after (b) treatment with Cr(VI) solution.
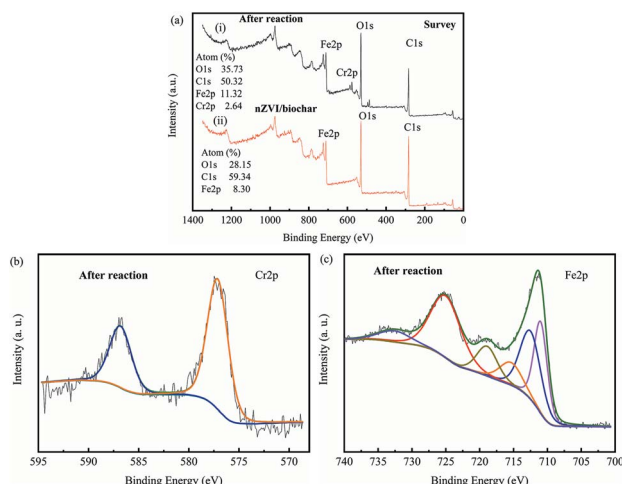

Fig. 12 XPS survey (a) for (i) nZVI/BC, (ii) after reaction with Cr(VI) solution and high-resolution XPS spectra for Cr 2p (b), Fe 2p (c) in nZVI/BC after reaction with Cr(VI) solution.

5 Conclusions

In this study, nZVI/BC was successfully synthesized by a one-step pyrolysis of Fe(III)-impregnated corn stover under a nitrogen atmosphere. The most probable pore size for nZVI/BC was about 50 nm. TEM imaging showed that the nZVI were well-scattered in the biochar. Then, the as-prepared nZVI/BC was applied in the Cr(VI) removal from aqueous solutions. It was found that the removal efficiency for Cr(VI) decreased with the increase in the initial pH value of the Cr(VI) solution in the

range of 4.0–10.0. The Cr(VI) concentration decreased rapidly from 10 to 0.046 mg L^{-1} in the first few minutes and then reached equilibrium (near 0) after 30 min. The Cr(VI) adsorption kinetics effectively followed a pseudo-second-order expression and the adsorption isotherm data were well fitted by the Langmuir model. The results of the XRD and XPS indicated that the adsorption mechanism included the Cr(VI) reduction accompanied by nZVI oxidation. The thermodynamic analysis showed that the Cr(VI) adsorption process by nZVI/BC is spontaneous and a high temperature is more favourable. These results demonstrate that nZVI/BC synthesized by a one-step carbothermal method can behave as a potential adsorbent for Cr(VI)-containing water treatment.

Conflicts of interest

The authors declare no conflicts of interest.

Acknowledgements

References

1 B. Dhal, H. N. Thatoi, N. N. Das and B. D. Pandey, *J. Hazard. Mater.*, 2013, **250–251**, 272.
2 A. Zhitkovich, *Chem. Res. Toxicol.*, 2011, **24**, 1617.
3 C. E. Barrera-Díaza, V. Lugo-Lugo and B. Bilyeu, *J. Hazard. Mater.*, 2012, **223–224**, 1.
4 T. K. Voa, H. K. Parkb, C. W. Namb, S. D. Kimb and J. Kima, *J. Ind. Eng. Chem.*, 2018, **60**, 485.
5 G. Qu, L. Kou, T. Wang, D. Liang and S. Hu, *J. Environ. Manage.*, 2017, **201**, 378.
6 A. Nam, U. S. Choi, S. T. Yun, J. W. Choi, J. A. Park and S. H. Lee, *J. Ind. Eng. Chem.*, 2018, **66**, 187.
7 Y. Zou, X. Wang, A. Khan, P. Wang, Y. Liu, A. Alsaedi, T. Hayat and X. Wang, *Environ. Sci. Technol.*, 2016, **50**, 7290.
8 F. Ogataa, E. Uetaa and N. Kawasakia, *J. Ind. Eng. Chem.*, 2018, **59**, 56.

9 W. Zhang, *J. Nanopart. Res.*, 2003, **5**, 323.

10 Y. Fang, J. Wen, G. Zeng, M. Shen, W. Cao, J. Gong and Y. Zhang, *Environ. Sci. Pollut. Res.*, 2018, **25**, 6175.

11 Y. Li, Z. Jin, T. Li and Z. Xiu, *Sci. Total Environ.*, 2012, **421–422**, 260–266.

12 Y. Y. Zhang, H. Jiang, Y. Zhang and J. F. Xie, *Chem. Eng. J.*, 2013, **229**, 412.

13 F. Fu, J. Ma, L. Xie, B. Tang, W. Han and S. Lin, *J. Environ. Manage.*, 2013, **128**, 822.

14 H. Zhu, Y. Jia, X. Wu and H. Wang, *J. Hazard. Mater.*, 2009, **172**, 1591.

15 H. Dong, J. Deng, Y. Xie, C. Zhang, Z. Jiang, Y. Cheng, K. Hou and G. Zeng, *J. Hazard. Mater.*, 2017, **332**, 79.

16 W. Gwenzi, N. Chaukura, C. Noubactep and F. N. D. Mukome, *J. Environ. Manage.*, 2017, **197**, 732.

17 L. Qian, W. Zhang, J. Yan, L. Han, Y. Chen, D. Ouyang and M. Chen, *Environ. Pollut.*, 2017, **223**, 153.

18 Y. F. Su, Y. L. Cheng and Y. H. Shih, *J. Environ. Manage.*, 2013, **129**, 361.

19 S. H. Ho, S. Zhu and J. S. Chang, *Bioresour. Technol.*, 2017, **246**, 123.

20 P. Wang, L. Tang, X. Wei, G. Zeng, Y. Zhou, Y. Deng, J. Wang, J. Wang, Z. Xie and W. Fang, *Appl. Surf. Sci.*, 2017, **392**, 391.

21 M. Lawrinenko, D. A. Laird and J. H. van Leeuwen, *ACS Sustainable Chem. Eng.*, 2017, **5**, 767.

22 R. Li, J. J. Wang, L. A. Gaston, B. Zhou, M. Li, R. Xiao, Q. Wang, Z. Zhang, W. Liang, H. Huang and X. Zhang, *Carbon*, 2018, **129**, 674.

23 R. He, Z. Peng, H. Lyu, H. Huang, Q. Nan and J. Tang, *Sci. Total Environ.*, 2018, **612**, 1177.

24 H. Liu, M. Li, T. Chen, C. Chen, N. S. Alharbi, T. Hayat, D. Chen, Q. Zhang and Y. Sun, *Environ. Sci. Technol.*, 2017, **51**, 9227.

25 F. Magalhães, M. C. Pereira, J. D. Fabris, S. E. C. Bottrel, M. T. C. Sansiviero, A. Amaya, N. Tancredi and R. M. Lago, *J. Hazard. Mater.*, 2009, **165**, 1016.

26 S. Wang, Y. Zhou, B. Gao, X. Wang, X. Yin, K. Feng and J. Wang, *Chemosphere*, 2017, **186**, 495.

27 S. Lagergren, *K. Sven. Vetenskapsakad. Handl.*, 1898, **24**, 1.

28 Y. S. Ho and G. McKay, *Process Saf. Environ. Prot.*, 1998, **76**, 332.

29 H. A. Toylor and N. Thon, *J. Am. Chem. Soc.*, 1952, **74**, 4169.

30 W. J. Jr Weber and J. C. Morris, *J. Sanit. Eng. Div., Am. Soc. Civ. Eng.*, 1963, **89**, 31.

31 I. Langmuir, *J. Am. Chem. Soc.*, 1918, **40**, 1361.

32 H. M. F. Freundlich, *Z. Phys. Chem.*, 1906, **57**, 385.

33 H. Gu, H. Lou, D. Ling, B. Xiang and Z. Guo, *RSC Adv.*, 2016, **6**, 110134.

34 H. T. Fan, X. Fan, J. Li, M. Guo, D. Zhang, F. Yan and T. Sun, *Ind. Eng. Chem. Res.*, 2012, **51**, 5216.

35 H. Yao, Q. Ding, H. Zhou, Z. Zhao, G. Liu and G. Wang, *RSC Adv.*, 2016, **6**, 27039.

36 C. H. Xu, L. J. Zhu, X. H. Wang, S. Lin and Y. M. Chen, *Water, Air, Soil Pollut.*, 2014, **225**, 1845.

37 H. Dang, Y. Zhang and P. Du, *Water Sci. Technol.*, 2014, **78**, 1398.

38 S. Zhou, Y. Li, J. Chen, Z. Liu, Z. Wang and P. Na, *RSC Adv.*, 2014, **92**, 50699.

39 H. Dong, Y. Zeng, G. Zeng, D. Huang, J. Liang, F. Zhao, Q. He, Y. Xie and Y. Wu, *Sep. Purif. Technol.*, 2016, **165**, 86.

40 R. Fu, Y. Yang, Z. Xu, X. Zhang, X. Guo and D. Bi, *Chemosphere*, 2015, **138**, 726.

41 Y. Li, W. Cheng, G. Sheng, J. Li, H. Dong, Y. Chen and L. Zhu, *Appl. Catal., B*, 2015, **174–175**, 329.

42 J. Shang, M. Zong, Y. Yu, X. Kong, Q. Du and Q. Liao, *J. Environ. Manage.*, 2017, **197**, 331.

43 M. S. H. Mak, I. M. C. Lo and T. Liu, *Water Res.*, 2011, **45**, 6575.

44 P. Yang, D. Guo, Z. Chen, B. Cui, B. Xiao, S. Liu and M. Hu, *J. Dispersion Sci. Technol.*, 2017, **38**, 1665.

45 J. H. Kim, J. H. Kim, V. Bokare, E. J. Kim, Y. Y. Chang and Y. S. Chang, *J. Nanopart. Res.*, 2012, **14**, 1010.

46 I. H. Yoon, S. Bang, K. W. Kim, M. G. Kim, S. Y. Park and W. K. Choi, *Environ. Sci. Pollut. Res.*, 2016, **23**, 1081.

47 X. Xia, L. Ling and W. X. Zhang, *Chemosphere*, 2017, **168**, 1597.